Adv. Polar Upper Atmos. Res., 14, 12–33, 2000

Interhemispheric conjugacy of auroral poleward expansion observed by conjugate imaging riometers at ~67° and 75°–77° invariant latitude

Hisao Yamagishi[1], Yuiti Fujita[2], Natsuo Sato[1], Masanori Nishino[3], Peter Stauning[4], Ruiyuan Liu[5] and Th. Saemundsson[6]

[1]*National Institute of Polar Research, Kaga 1-chome, Itabashi-ku, Tokyo 173-8515*
[2]*Nagano JRC Co., Shimo Higano, Inasato-cho, Nagano 381-2211*
[3]*Solar-Terrestrial Environment Laboratory, Nagoya University, Honohara, Toyokawa 442-8507*
[4]*Danish Meteorological Institute, Lyngbyvej 100, Copenhagen O, Denmark*
[5]*Polar Research Institute of China, 451 Jinqiao Road, Shanghai 200129, China*
[6]*Science Institute, University of Iceland, Dunhaga 3, Reykjavik 103, Iceland*

Abstract: Interhemispheric conjugacy of auroral poleward expansion was studied using conjugate imaging riometers at ~67° inv. (invariant latitude) (Syowa Station, Antarctica, and Tjornes, Iceland) and at 75–77° inv. (Zhongshan Station, Antarctica; Longyearbyen, Svalbard and Danmarkshavn, Eastern Greenland). Ninety poleward expansion events at ~67° inv. observed in 1992–1993 were analyzed. The expansion at this latitude was characterized by a continuous poleward motion of cosmic noise absorption (CNA) bands with a velocity distribution that peaked at 1–1.5 km/s at a polar ionospheric altitude of ~90 km. The velocity distribution has another apparent peak at 3–5 km/s when measurements are made along the meridian. However, ~60% of the events forming this peak are overestimated because the motion of the CNA region's front was observed while the front was tilted away from the east-west direction. The difference in expansion velocities between conjugate stations remained within ±30% for half of the events. The time lag between the passage of a CNA band over conjugate stations was typically between 30–60 s. The product of this time lag and the poleward expanding velocity provides the location of the actual conjugate point. For 87% of the total number of events, the conjugate point for Syowa was located within ±200 km of Tjornes.

The poleward expansion observed at 75°–77° inv. was characterized by a stepwise progression of CNA bands to higher latitudes. In other words, new CNA bands formed 50–180 km poleward of the preceding CNA band. The appearance of a new CNA band was often associated with an equatorward motion of the preceding CNA band. Equatorward moving CNA bands are thought to be located in a closed fieldline. The persistence of this band for several minutes was explained by pitch angle scattering of the trapped electrons as a result of a very stretched fieldline configuration in which the fieldline curvature was comparable to the Larmor radius of the trapped electrons.

Although the conjugate pair used at these latitudes was displaced longitudinally by ~500 km, conjugacy was generally good. If a time lag of ±15 min is allowed, 52% of the CNA events observed at Longyearbyen had a counterpart at Zhongshan, and 40% had a counterpart at Danmarkshavn. This rather high level of conjugacy suggests that the characteristic longitudinal extent of the poleward expanding CNA bands is on the order of 500 km in the polar ionosphere.

1. Introduction

Several concepts have been used to explain the onset and expansion of substorms. The near-earth picture consists of a thin current sheet formation (*e.g.*, Sergeev *et al.*, 1993), the disruption of a cross-tail current, and a current wedge formation (McPherron *et al.*, 1973). The far-tail picture consists of magnetic fieldline reconnection and the ejection of a plasmoid (*e.g.*, Hones *et al.*, 1984). However, the timing and causality of near-earth and far-tail processes at the onset of a substorm are controversial (*e.g.*, Birn and Hesse, 1991; Lui, 1991). Multi-satellite observations in the magnetotail are useful for answering this kind of question. However, the satellites must be positioned at appropriate locations in the tail at the onset of the substorm. Since the onset and expansion of a substorm are projected in the polar ionosphere as an auroral display, the observation of a poleward expanding aurora by a chain of ground-based aurora imagers (*e.g.*, Sergeev and Yahnin, 1979) is a useful method for obtaining a global view of the substorm to complement single-point satellite observations.

Opportunities for optically observing auroras from a chain of ground stations are very limited because optical observations are not possible in the summertime and because the sky is rarely clear at every station in the chain. The use of radiowaves to observe auroras is a good solution to this problem, enabling auroras to be observed in all seasons and under all weather conditions. The imaging riometer was first developed by Detrick and Rosenberg (1990) and was soon installed in observation stations throughout the arctic and antarctic regions (Stauning, 1996). This instrument observes the aurora as a cosmic noise absorption (CNA) image. Although the spatial resolution of an imaging riometer is relatively poor (typically ~20 km) compared to that of optical instruments, the riometer has several advantages. First, auroras can be observed at any time of day or night, even if the sky is cloudy. Secondly, riometers are sensitive to the precipitation of energetic electrons over a range of several tens of keV. In an auroral poleward expansion event, these electrons are produced by reconnection processes in the magnetotail. Images of this type of precipitation provide useful information on where and how reconnection is occurring in the magnetotail. On the other hand, optical imagers are sensitive to the precipitation of electrons over a range of several keV, providing information on field-aligned potential structures that accelerate auroral electrons.

Stauning *et al.* (1995) were the first to use an imaging riometer network, together with a chain of magnetometers and normal riometers, to analyze poleward expansion. They showed that the poleward expansion, as viewed by CNA images, did not appear as a smooth motion, but as a series of stepwise intensification of CNA. Hargreaves *et al.* (1997) analyzed substorm-associated nightside absorption spikes using an imaging riometer at the South Pole (74.1° invariant latitude [inv.]) and Kilpisjaervi (65.9° inv.). Their absorption spikes were very similar to what we call poleward expanding CNA bands in this paper, with the same spatial form, velocity, direction and duration.

In this paper, we analyze poleward expanding CNA events that were observed using conjugate imaging riometer stations at two geomagnetic latitudes: ~67° inv. (Syowa Station, Antarctica, and Tjornes, Iceland) and 75°–77° inv. (Zhongshan Station, Antarctica; Longyearbyen, Svalbard; and Danmarkshavn, Eastern Greenland). We attempted to compare the morphology of the poleward expansion at latitudes near the

start and end points of the expansion. The conjugacy of poleward expanding CNA events at ~67° has been studied by Fujita *et al.* (1998) using the same data set, but with the intention of analyzing the seasonal variations in the conjugate point's position.

2. Conjugate imaging riometer observations

2.1. Imaging riometer stations

A pair of imaging riometers was installed in Iceland in July 1990 and at Syowa Station in February, 1992. This system provides CNA images of auroras at conjugate points throughout the year with an 8×8 pixel resolution (~20 km per pixel). In the middle of the 1990s, the network was extended to include higher latitudes from Eastern Greenland to Svalbard and their conjugate regions in Antarctica, as shown in Table 1. Figure 1a shows the locations of the arctic riometer stations (LYB: Longyearbyen, Svalbard; DMH: Danmarkshavn, Eastern Greenland; TJO: Tjornes, Iceland) together with their fields of view. The conjugate antarctic riometer stations (ZHS: Zhongshan Station; SYO: Syowa Station) and their fields of view are also shown in the figure.

Table 1. Imaging riometers used in the present study.

Station	Lat.	East Lon.	Inv. Lat.	Installation	Participating organization
Tjornes	66.20	−17.12	66.7	July 1990	NIPR
Syowa Station	−69.00	39.58	66.1	Feb. 1992	NIPR
Danmarkshavn	76.77	−18.66	77.3	Sep. 1992	DMI, NIPR
Longyearbyen	78.20	15.80	75.1	Aug. 1995	DMI, NIPR, UNIS
Zhongshan Station	−69.37	76.38	74.7	Jan. 1997	NIPR, STEL, PRIC

NIPR: National Institute of Polar Research.
DMI: Danish Meteorological Institute. UNIS: University Course in Svalbard.
STEL: Solar Terrestrial Environment Lab., Nagoya University.
PRIC: Polar Research Institute of China.

The specifications of the riometers are slightly different. The operating frequency is 30 MHz for Syowa and Tjornes stations, and 38.2 MHz for the other stations. The separation of each dipole antenna in the phased array is 0.65 wavelengths for Syowa and Tjornes stations, 0.55 wavelengths for Danmarkshavn station, and 0.5 wavelengths for Longyearbyen and Zhongshan stations. Accordingly, the size of the field of view is 200 km by 200 km for Syowa and Tjornes stations, 250 km by 250 km for Danmarkshavn station, and 300 km by 300 km for Longyearbyen and Zhongshan stations.

2.2. Model calculation of the conjugate point at ~67° inv.

Geomagnetically conjugate points can be calculated by fieldline tracing from a point in one hemisphere to the opposite hemisphere. In the fieldline tracing for high latitude stations, not only the earth's internal field, but also the external field caused by magnetospheric currents must be taken into consideration. The reason for this is that the field line extends deep into the magnetosphere, where the magnetic field intensity from internal origins becomes comparable to that of the external origins. In our calculation, the

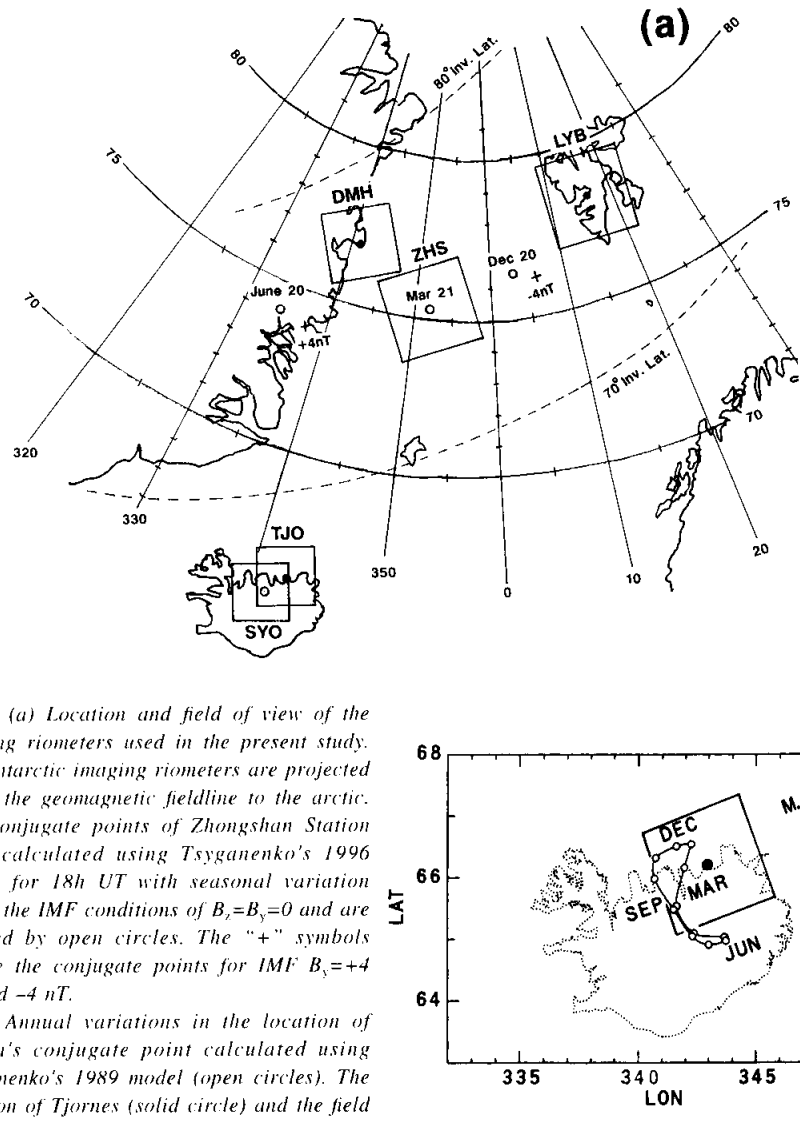

Fig. 1. (a) Location and field of view of the imaging riometers used in the present study. The antarctic imaging riometers are projected along the geomagnetic fieldline to the arctic. The conjugate points of Zhongshan Station were calculated using Tsyganenko's 1996 model for 18h UT with seasonal variation under the IMF conditions of B_z=B_y=0 and are marked by open circles. The "+" symbols denote the conjugate points for IMF B_y=+4 nT and -4 nT.

(b) Annual variations in the location of Syowa's conjugate point calculated using Tsyganenko's 1989 model (open circles). The location of Tjornes (solid circle) and the field of view of the riometer (open square) are also shown.

IGRF 95 model was used for the internal field, and the Tsyganenko 1989 model (Tsyganenko, 1990) was used for the external magnetic field. Figure 1b shows the conjugate points of Syowa calculated for each month of the year at magnetic midnight, as marked by the small open circles. The location of Tjornes and the view field of the riometer are also marked in the figure with a solid circle and an open square, respectively. The conjugate point of Syowa is located poleward of Tjornes in November, December and January; at the same geomagnetic latitude in October and February; and equatorward of Tjornes for the rest of the year.

2.3. Model calculation of the conjugate point at 75°–77° inv.

In this latitude range, the geomagnetic fieldlines are connected to the interplanetary magnetic field near noon and midnight local time, and a conjugate point cannot be defined. Except for these time periods, the conjugate point can be obtained by fieldline tracing using Tsyganenko's 1996 model (Tsyganenko and Stern, 1996) up to an invariant latitude of ~77°. Three open circles with the dates in Fig. 1a denote the conjugate point of Zhongshan at 18h UT for the vernal equinox, winter and summer solstices under the interplanetary magnetic field (IMF) conditions of B_z=B_y=0. Two "+" marks denote the conjugate point of Zhongshan at 18h UT on March 21 under the IMF conditions of B_y= + 4 nT and − 4 nT. The conjugate point of Zhongshan moves much more than that of Syowa. However, this network can be used for a conjugate study because the conjugate point of Zhongshan moves between Longyearbyen and Danmarkshavn and is in conjugacy with one of these stations most of the time.

3. Conjugacy of poleward expansion at ~67° inv.

3.1. Typical poleward expansion on February 18, 1993

Figure 2a shows a typical example of poleward expansion observed by the imaging riometers at Tjornes (upper panel) and Syowa Station (lower panel) on February 18, 1993, during the time interval of 2059–2101 UT (after Fujita *et al.*, 1998). Magnetic local time is almost equal to UT for Syowa and Tjornes. A CNA band elongated in a geomagnetically east-west direction was observed moving poleward by both stations. It must be noted that the CNA band at Tjornes was located at a lower latitude than that of Syowa. To overlap the CNA bands seen from both stations, Syowa field of view must be shifted equatorward. This means that the actual conjugate point of Syowa was located equatorward of Tjornes. Note that poleward expansion at Syowa occurred more rapidly between 2059:31 and 2100:03 than it did at Tjornes. A meridional display of the CNA in Fig. 2b shows this feature more clearly. The white bands rising to higher latitudes correspond to poleward expanding CNA bands. The black lines in the white bands are fitted curves showing the poleward expansion velocities; the expansion velocity was calculated as 2.8 km/s for Syowa and 1.7 km/s for Tjornes. The moment at which the CNA band passed overhead is marked by a "+" in the meridional display; the time of overhead passage was 2059:41 UT for Syowa and 2100:24 UT for Tjornes. The time lag in the overhead passage (Tjornes lagged by 43 s) and the velocity of the poleward expansion (1.7 km/s) shows that the location of Tjornes is 73 km poleward of the conjugate point for Syowa in this particular case.

3.2. Statistics of poleward expansion features observed during 1992–1993

We selected 90 events of poleward expanding CNA bands observed simultaneously at Syowa and Tjornes based on the following criteria:

(1) The CNA intensities at either station must be larger than 1 dB at their maximum to ensure that only pronounced CNA events are included in the analysis.

(2) The time lag between the overhead passage of the CNA bands must be less than 300 s.

(3) The onset of the event of interest must not be preceded by a similar CNA event for at

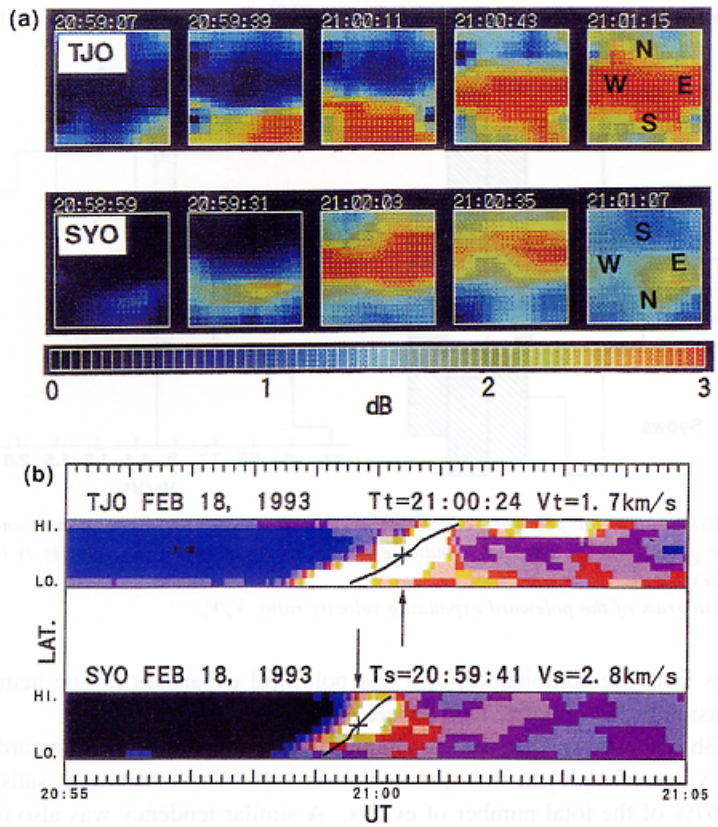

Fig. 2. (a) Typical example of a poleward expanding CNA event observed at Tjornes (upper panel) and Syowa Station (lower panel) on February 18, 1993.
(b) Meridional display of the above event (after Fujita et al., 1998).

least 30 min to avoid confusion.

Figure 3a shows a histogram of the poleward expanding velocities measured at Tjornes (V_t; upper panel) and Syowa (V_s; lower panel). The distribution has two peaks for both stations; one at 1–1.5 km/s and the other at 3–5 km/s. The latter peak includes events in which the poleward expanding velocity was overestimated because the motion of the tilted CNA region was observed using meridional beams. These events are indicated by the hatched area in Fig. 3a. If these events are removed, the velocity distribution is no longer bimodal. Instead, the distribution has a single peak at 1–1.5 km/s. This phenomenon is discussed in more detail in Section 5.1.

Figure 3b shows a histogram of the poleward expanding velocity ratio, V_s/V_t, calculated for each event. A major peak occurs at $0.9<V_s/V_t<1.1$, and a minor peak occurs at $1.5<V_s/V_t<3.7$. The former peak shows that the conjugacy between Syowa and Tjornes is fairly good. Events with a velocity difference of less than ±10% ($0.9<V_s/V_t<1.1$) account for 20% of the total. Forty-five percent of all events have a velocity difference within ±30% ($0.77<V_s/V_t<1.3$). The broad distribution of V_s/V_t from 0.27 to

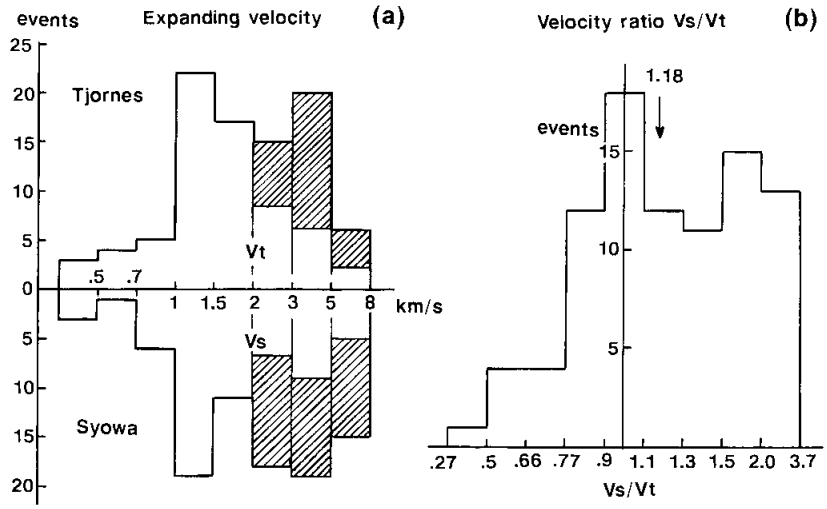

Fig. 3. *(a) Histogram of the poleward expanding velocity at Tjornes (V_t; upper panel) and Syowa (V_s; lower panel). The hatched area indicates those events in which the velocity is overestimated (see text).*
(b) Histogram of the poleward expanding velocity ratio, V_s/V_t.

3.7 originates from the combination of a fast poleward expansion in one hemisphere and a slow expansion in the opposite hemisphere.

Figure 3b also shows that the distribution has a noticeable bias towards $V_s/V_t > 1$. The median value of V_s/V_t in this distribution is 1.18. The events that satisfy $V_s/V_t > 1$ account for 67% of the total number of events. A similar tendency was also observed for optical observations of auroras. Sato and Saemundsson (1987) reported a case in which the poleward expanding velocity at Syowa was 1.7 times faster than that in Iceland. Fujita *et al.* (1998) presented a possible reason for the higher expanding velocity at Syowa using a geomagnetic fluxtube model to connect the conjugate points. A smaller inclination angle and a weaker total field at Syowa causes the diameter of the fluxtube to be 11% larger than that at Tjornes. This means that when a source region of the CNA moves in the magnetic equatorial plane, the projection of the region's motion is 11% larger at Syowa than that at Tjornes.

Figure 4a shows a histogram of the time lag between the overhead passage ($T_s - T_t$) of the CNA band at Syowa ($t=T_s$) and Tjornes ($t=T_t$). A positive time lag ($T_s - T_t > 0$) corresponds to a situation where the CNA band passed over Tjornes before it passed over Syowa. This means that the conjugate point of Syowa was located poleward of Tjornes. A negative time lag ($T_s - T_t < 0$) corresponds to a situation where the conjugate point of Syowa was located equatorward of Tjornes. Clear peaks in the time-lag distribution can be seen at 30–60 s and $-30 \sim -60$ s. If these time lags are multiplied by the poleward expanding velocity shown in Fig. 3a, the location of the conjugate point can be determined. Figure 4b shows a histogram of the calculated meridional distance of the conjugate point from Tjornes (positive=poleward). The distribution is slightly asymmetric, *i.e.*, the Syowa conjugate point was more often located equatorward of Tjornes than poleward. This feature is consistent with the results of the theoretical

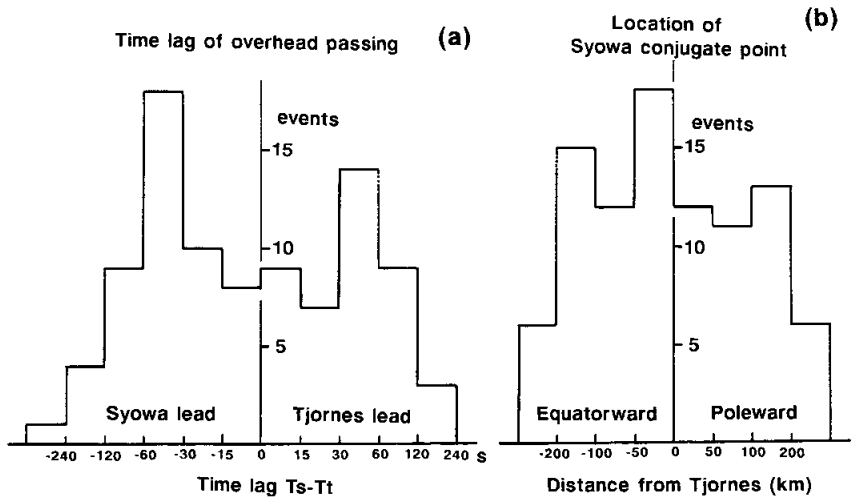

Fig. 4. *(a) Histogram of the time lag between the overhead passage of CNA bands over Syowa and Tjornes.*
(b) Histogram of the meridional distance between the conjugate point of Syowa and Tjornes.

calculations shown in Fig. 1b, where the conjugate point of Syowa is located equatorward of Tjornes for more than half the year.

4. Conjugacy of poleward expansion at 75°–77° inv.

To study the conjugate features of poleward expanding CNAs in the 75°–77° inv. range, we selected two conjugate CNA events: one at a quiet time and the other at an active time.

4.1. CNA event on May 17, 1998

According to IMAGE magnetometer array data, this event was not a substorm, but a small high-latitude magnetic disturbance centered at 75° inv. No notable injection was found at a synchronous orbit during this event. Figure 5 shows a series of CNA images observed at Longyearbyen (right panels) and Zhongshan Station (left panels) during the periods of 1750–1814 UT and 1828–1838 UT, with an image interval of 32 s. In the CNA images from both stations, up corresponds to poleward and right to magnetic east. Several CNA forms, labeled A to F, are found in the field of view of Longyearbyen and/or Zhongshan. The shape, location and motion of these CNA activities are schematically illustrated in Fig. 6, with the time interval of their appearance in UT. Note that the field of view of the Zhongshan riometer is projected towards the northern hemisphere and located a little equatorward of Longyearbyen. A description of each CNA activity follows.

Activity A (1750–1755 UT): A folded CNA band of ~1 dB, labeled A, was seen in Longyearbyen's field of view. No notable movement of this band was observed.

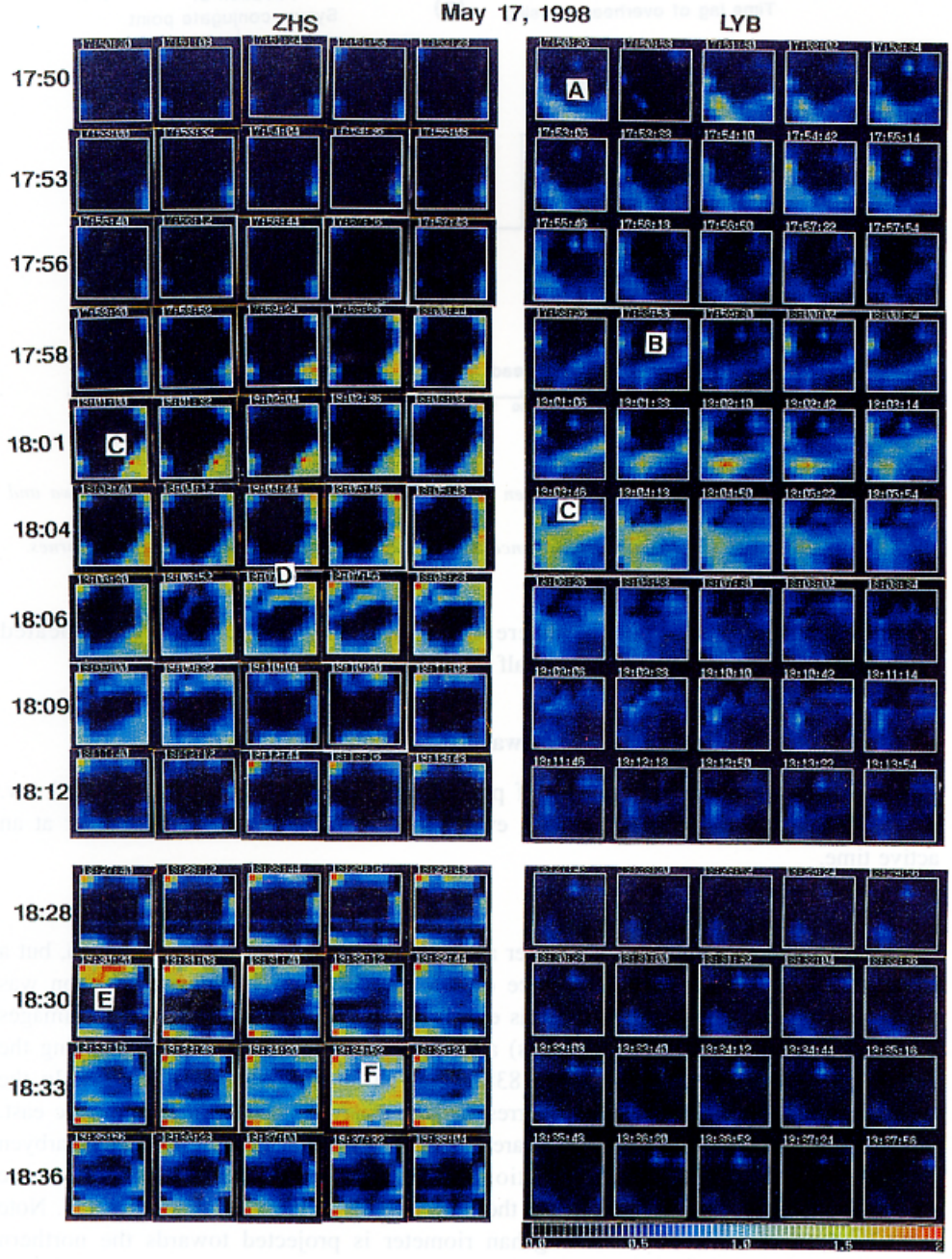

Fig. 5. Series of CNA images observed at Longyearbyen (right panel) and Zhongshan (left panel) at 1750–1838 UT on May 17, 1998.

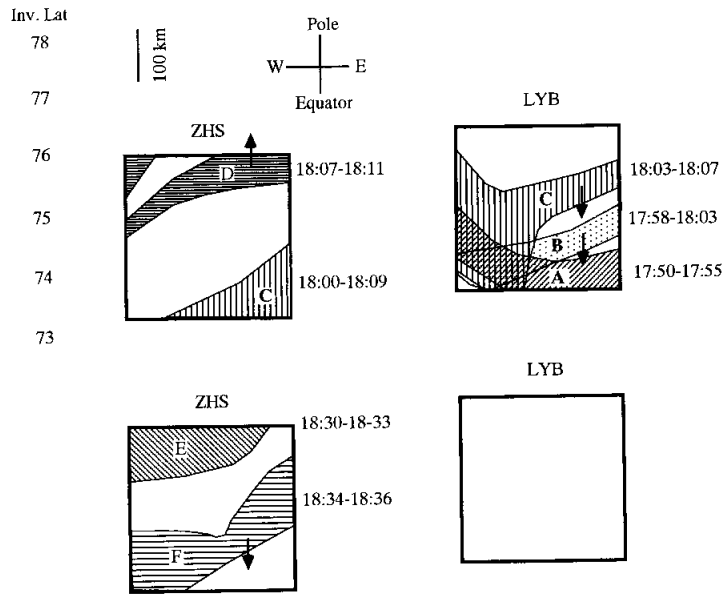

Fig. 6. Schematic illustrations of the CNA event on May 17, 1998.

Activity B (1758–1803 UT): At Longyearbyen, a CNA band of 0.8 dB, labeled B, appeared ~50 km poleward of A's previous position. B moved equatorward and intensified up to 1.8 dB at 1802 UT. The CNA activity at the bottom right corner of the Zhongshan field of view may be a continuation of this activity.

Activity C (1803–1807 UT): A CNA band of 1.5 dB, labeled C, appeared at Longyearbyen ~100 km poleward of B's previous position and moved equatorward. The CNA activity at the bottom right corner of the Zhongshan field of view may be a continuation of this activity.

Activity D (1807–1811 UT): A CNA band of ~1.2 dB, labeled D, appeared at Zhongshan just after C faded at Longyearbyen.

Activity E (1830–1833 UT): A CNA band of ~2 dB, labeled E, appeared at the top left corner of the Zhongshan field of view.

Activity F (1834–1835 UT): A CNA band of 1.5 dB, labeled F, appeared at Zhongshan ~180 km equatorward of E's previous position and moved equatorward.

During some of these activities, the CNA bands moved equatorwards at a speed of ~0.5 km/s. This equatorward motion was followed by the appearance of a new CNA band at 50–180 km poleward of the preceding CNA activity (*e.g.*, the appearance of C after equatorward motion of B; the appearance of D after the equatorward motion of C).

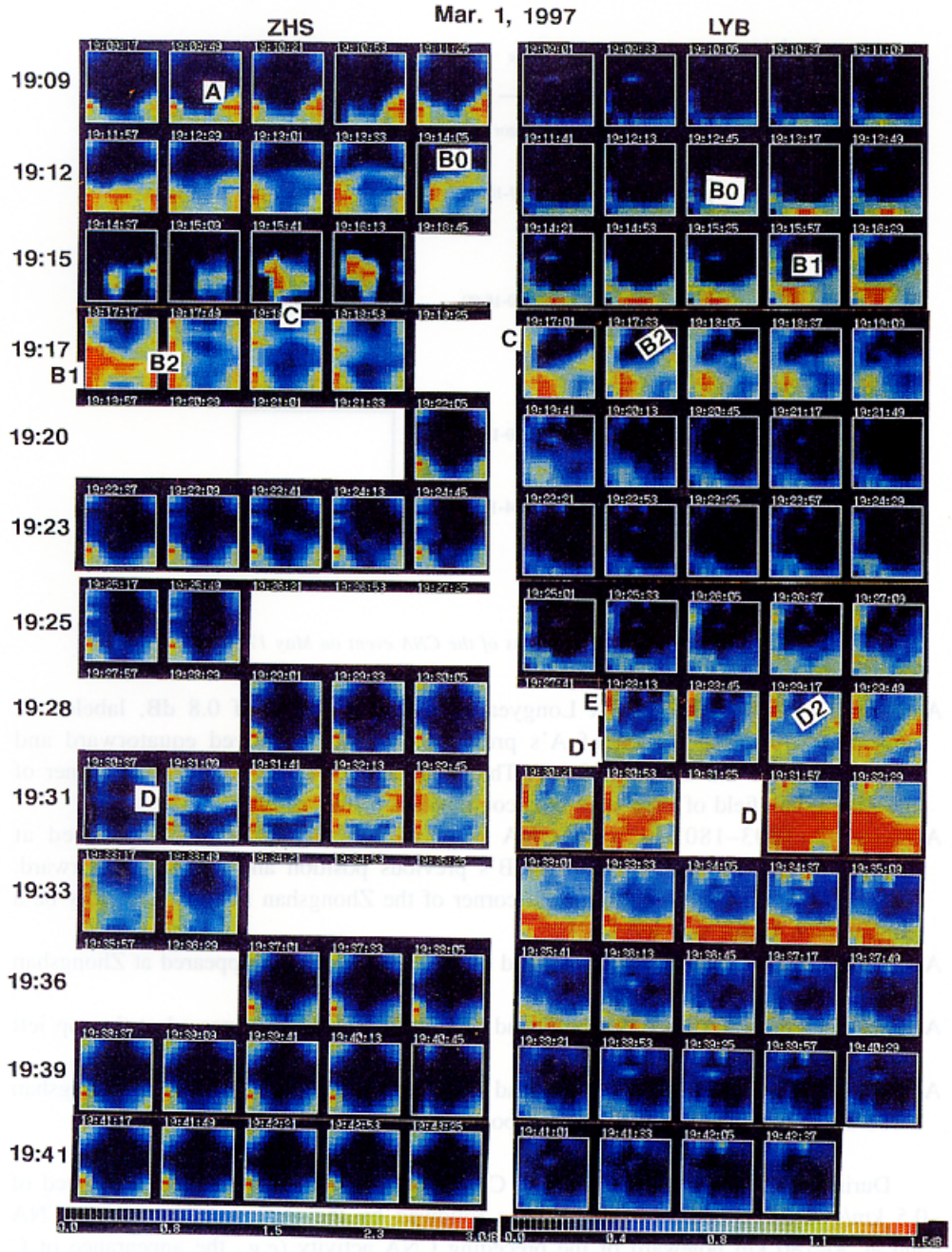

Fig. 7. Series of CNA images observed at Longyearbyen (right panel) and Zhongshan (left panel) at 1909–1943 UT on March 1, 1997.

4.2. CNA event on March 1, 1997

The IMAGE magnetometer array data shows that the magnetic disturbance causing this CNA event started at 71° inv. at 1840 UT, expanded poleward beyond 76° inv., and then returned equatorwards. The highest latitude excursion occurred at ~1918 UT. Small injections of 50–225 keV electrons were observed at 1902 and 1914 UT at a synchronous orbit near midnight.

Figure 7 shows a series of CNA images observed at Longyearbyen (right panel) and Zhongshan (left panel) at 1909–1943 UT on March 1, 1997.

Several CNA images are missing from Zhongshan set of data. At these times, the riometer data was contaminated by noise from a digital ionosonde at the station. The CNA images from 1915 to 1916 UT are also contaminated by this noise. Figure 8 shows the images observed at Danmarkshavn at 1925–1943 UT on the same day. Several CNA forms, labeled A to F, are found in the fields of view of these three stations. The shape, location and motion of these CNA activities are schematically illustrated in Fig. 9

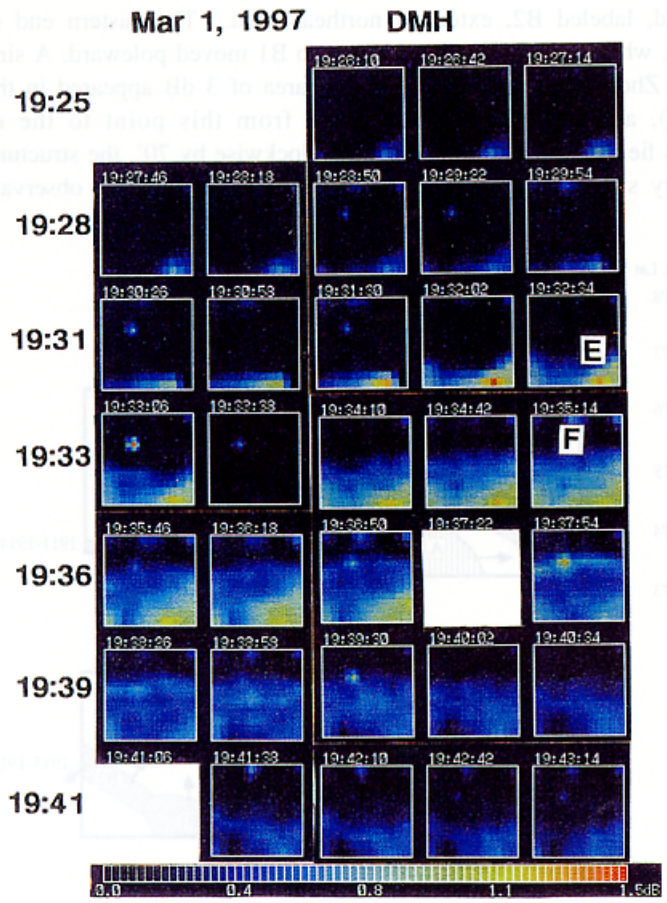

Fig. 8. Series of CNA images observed at Danmarkshavn at 1925–1943 UT on March 1, 1997.

(Longyearbyen and Zhongshan, 1909–1919 UT) and Fig. 10 (Longyearbyen, Zhongshan and Danmarkshavn, 1925–1943 UT), with the time of their appearance in UT.

Some of the CNA activities observed at the different stations seem to have the same source, judging from their simultaneous appearance, similar direction of motion, and common inv. range. In such cases, the common CNA activities at different stations are labeled with the same symbol. A description of each CNA activity follows.

Activity A (1909–1912 UT in Figs. 7 and 9): A CNA area of 3 dB, labeled A, was observed in the bottom right corner of the Zhongshan field of view. The area intensified and extended westward.

Activity B0 (1911–1914 UT in Figs. 7 and 9): A CNA band of 1.5–2 dB, labeled B0, appeared at Zhongshan ~100 km poleward of A's position and moved poleward. At the same time, the continuation of B0 was seen at the bottom of Longyearbyen's field of view.

Activity B1 and B2 (1915-1919 UT in Figs. 7 and 9): A CNA area of 1.5 dB, labeled B1, appeared in the bottom left corner of the Longyearbyen's field of view. From B1, a CNA band, labeled B2, extended northeastward. The eastern end of B2 moved equatorward, while the other end connected to B1 moved poleward. A similar structure was seen at Zhongshan at 1917 UT. CNA area of 3 dB appeared in the bottom left corner (B1), and a CNA band extended from this point to the east (B2). If Zhongshan's field of view is rotated counterclockwise by 70°, the structure of the CNA bands is very similar to that observed at Longyearbyen. These observations seem to

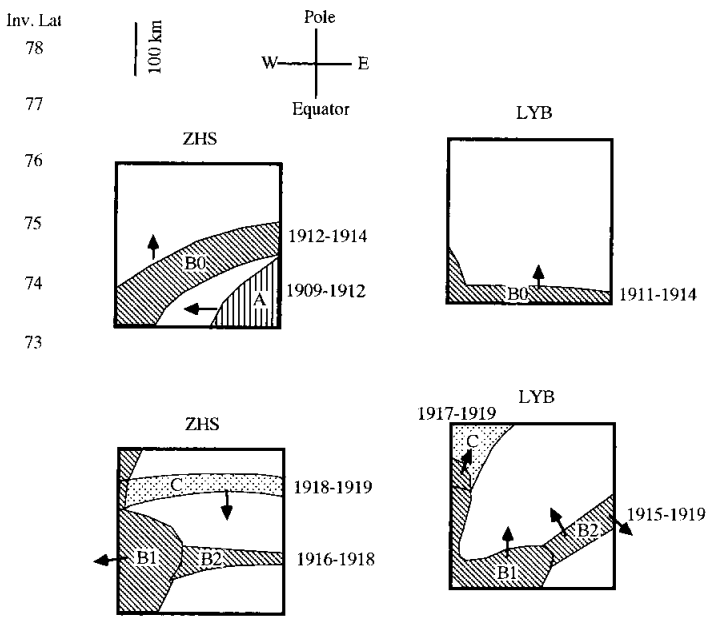

Fig. 9. Schematic illustrations of the CNA event observed at Longyearbyen and Zhongshan at 1911–1919 UT on March 1, 1997.

suggest the possibility that the conjugate point of Zhongshan was located close to Longyearbyen at this time and that both stations observed the same part of the CNA bands. The IMF B_y observed by the WIND satellite was −2~ −3 nT during this period, so the location of Zhongshan's conjugate point may have been near Longyearbyen (see the conjugate point for IMF $B_y = -4$ nT in Fig. 1a).

Activity C (1917–1919 UT in Figs. 7 and 9): When B1 and B2 faded at Zhongshan at 1917:49, a CNA band, labeled C, appeared ~100 km poleward of B2's position and moved equatorward. At the same time, a CNA area, labeled C, appeared at the top left corner of Longyearbyen's field of view at 1917 UT and lasted until 1919 UT.

Activity D1, D2 and E (1925–1930 UT in Figs. 7 and 10): After 5 min of no activity, a CNA region was activated at the bottom of Longyearbyen's field of view at 1925 UT, and then intensified in the bottom left corner (D1). A CNA band, labeled D2, extended northeastward from this point. Another CNA area of 0.8 dB, labeled E, appeared on the left at 1925 UT. E moved poleward and intensified at 1928 UT to reach 1.5 dB. Interestingly, the location of CNA areas D1, D2 and E at 1928–1930 looks very similar to B1, B2 and C at 1917–1919. This observation suggests that the location of the active areas in the magnetosphere remained fixed during the quiet period of 1920–1924 UT.

Activity D (1931–1943 UT in Figs. 7 and 10): D1 and D2 merged into D, and moved equatorward.

Activity E (1933–1938 UT in Figs. 7, 8 and 10): A CNA area, labeled E, was seen at the top of Longyearbyen's field of view. E moved poleward and nearly exited the field of view. A continuation of E was seen at the bottom right corner of Zhongshan's field of view, expanding poleward and westward.

Activity F and E (1933–1943 UT in Figs. 8 and 10): At Zhongshan, a CNA area of 0.8 dB, labeled F, appeared poleward of E at 1933 UT. During the interval of 1936–1937 UT, F expanded poleward, while E moved equatorward and faded out. After 1940 UT, F also retreated equatorward and faded.

As in the May 17 event, this case reveals a close relationship between the equatorward motion of a CNA band and the appearance of a new CNA band poleward of the preceding activity. For example, a close relationship was observed between the appearance of C and the equatorward motion of B2 at Longyearbyen as well as the appearance of E and the equatorward motion of D. The magnetospheric processes causing the above features will be discussed in Section 5.

4.3. Statistics of CNA conjugacy at 75°–77° inv.

After analyzing the above two conjugate CNA events, we have concluded that the imaging riometers at Longyearbyen, Danmarkshavn and Zhongshan did not necessarily observe the same CNA band, but may have observed different bands in adjacent activities. This hypothesis would explain the time lag of several minutes in the appearance of the CNA area at conjugate stations. To determine the probability of observing conjugate CNA events, we selected 85 CNA events observed at Longyearbyen during the period of January 27–April 7, 1997. Allowing a time lag of ±15 min, 52% of the CNA events had a counterpart at Zhongshan, and 40% had a counterpart at

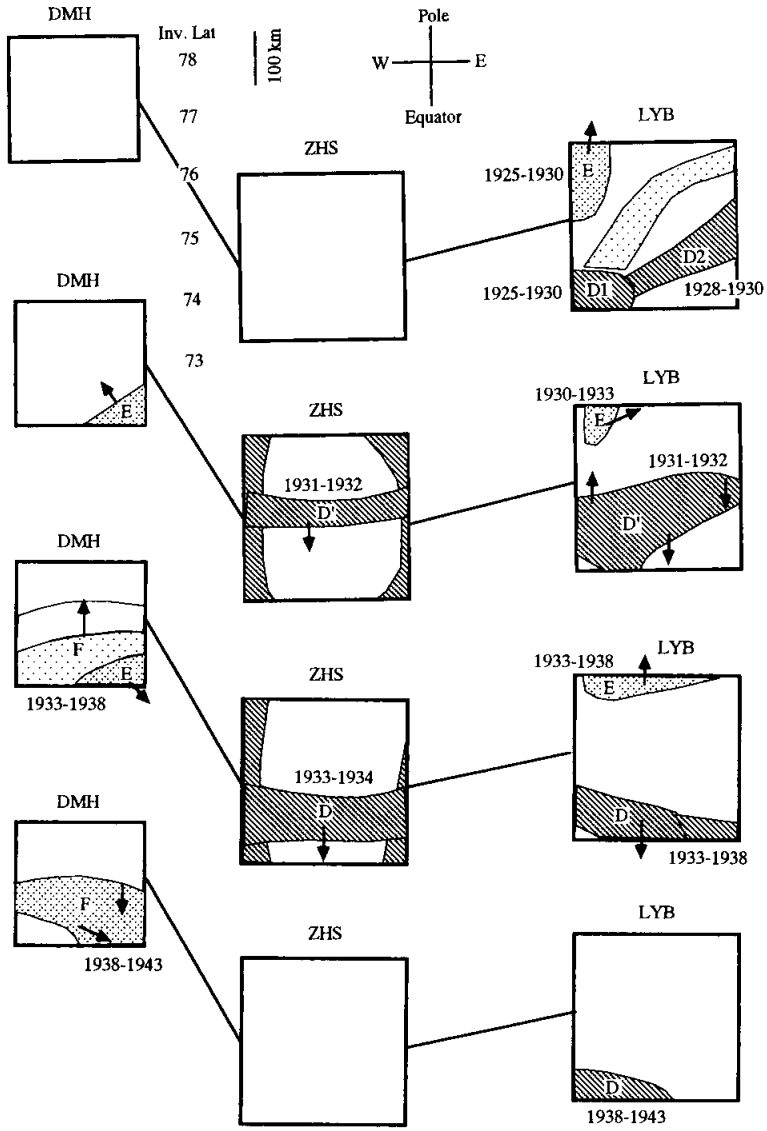

Fig. 10. Schematic illustrations of the CNA event observed at Longyearbyen, Zhongshan and Danmarkshavn at 1925–1943 UT on March 1, 1997.

Danmarkshavn. This rather high rate of conjugacy suggests that the characteristic longitudinal extent of poleward expanding CNA bands is on the order of 500 km in the polar ionosphere.

5. Discussions

5.1. Apparent bimodal distribution of the poleward expansion velocity at ~67° inv.

In Fig. 3a, two peaks are found in the poleward expansion velocity distribution: a slow expansion with a velocity of 1–1.5 km/s and a fast expansion with a velocity of 3–5 km/s. Similar velocities were reported in previous works of multi-beam and imaging riometer observations performed at this latitude (Nielsen, 1980; Hargreaves *et al.*, 1997). In our study, we determined the poleward expansion velocity not from CNA images, but from a meridional display of these images. We therefore checked the CNA images for any characteristic differences between the two expansion velocity groups. Most cases of slow expansion were well-defined poleward expansions with a clear CNA band extending in the east-west direction. The cases of fast expansion consisted of the following categories:

Group A (moving front of the CNA band is parallel to the east-west direction)
(A1) constant poleward motion of a CNA band (normal poleward expansion)
(A2) poleward leap of a CNA band
(A3) stepwise spread of a CNA band
Group B (moving front of the CNA band is tilted away from the east-west direction)
(B1) constant poleward motion of a CNA band extending in an oblique direction
(B2) passage of a westward travelling surge
(B3) radial expansion of a CNA region

Meridional beam observations enable the true poleward-moving velocity to be calculated for group A, while a larger apparent velocity is calculated for group B. When the angle between the front and the meridian becomes smaller, the poleward velocity obtained by the meridional beams appears larger than the actual value. The hatched area in Fig. 3a indicates the events included in group B. These events account for ~60% of the fast expansions. If we remove these events, the poleward expanding velocity distribution is no longer bimodal, but has a single peak at 1–1.5 km/s.

Kadokura *et al.* (1999) reported that the poleward expansion of auroral brightening during the onset of a substorm onset was initially fast (~5 km/s), but when the expansion reached a certain latitude it increased its scale and slowed (~1 km/s) its expansion. Since the field of view of the imaging riometer is limited (200 km by 200 km), the initial brightening is rarely caught. However, the possibility of observing a fast expansion near the initial area of brightening cannot be excluded.

5.2. Poleward expansion of CNA at 75°–77° inv.

5.2.1. Similarity to optical auroras

The formation of new arcs at the front of the expanding bulge is thought to be a typical phenomenon associated with strong substorm expansion at high latitudes (*e.g.*, Akasofu, 1965; Sergeev and Yahnin, 1979). De la Beaujardiere *et al.* (1994) analyzed the quiet-time intensification of aurora along the most poleward boundary of auroras near midnight. At the time of intensification once per hour, they found that the arc marking the poleward auroral boundary had intensified, and that a new arc had appeared poleward of this arc. The preceding arcs then drifted equatorward. A similar appearance and motion of auroras at the poleward boundary was reported for an active period (Pudovkin,

1991).

We observed the poleward expansion of CNA at 75°–77° inv. during both quiet and active times. In both cases, expansion consisted of the appearance of a new CNA band poleward of the preceding CNA band with the latter band moving equatorward just before or after the appearance of the new band. These features are very similar to the optical aurora observations described above. However, the similarities between optical auroras and the CNA at the auroral poleward boundary does not mean that the mechanism of both phenomena is the same, because CNA is caused by the precipitation of electrons of several tens of keV, while optical auroras are caused by electrons of several keV.

5.2.2. Equatorial source of poleward progressing CNA bands

When the CNA is much greater than 1 dB, it is usually ascribed to the precipitation of electrons of several tens of keV. During poleward expansion events, electrons in this energy range are produced by the reconnection process at a separatrix in the magnetotail. Some of these hot electrons precipitate directly into the polar ionosphere, causing CNA. The poleward progression of CNA bands can be explained by the continuous formation of a new separatrix just tailward of the preceding one.

5.2.3. Equatorward motion of preceeding CNA band

When a new CNA band appears on the poleward side, the preceding CNA band has usually moved equatorward and faded within several minutes. The energetic electrons causing this CNA band are probably not directly supplied from the separatrix, because a new separatrix must have formed further out in the tail to cause the precipitation resulting in the appearance of the poleward CNA band. Therefore, the equatorward retreating CNA band must be located in a closed fieldline region. Fieldlines connected to this CNA band change configuration from a very stretched pattern to a dipole-like shape. This dipolarization leads to the poleward motion at the foot of this fieldline, which is opposite to the observed motion of the CNA band. Therefore, the equatorward motion of the CNA band can only be explained by the earthward drift of hot electrons across an L-shell. At the time of reconnection, a strong dawn-to-dusk electric field (reconnection electric field) transiently appears. Anti-parallel magnetic fields at both sides of the neutral sheet and the reconnection electric field compress both lobes of the plasma into the neutral sheet. In the course of reconnection, hot plasma and a vertical component of the fieldline are produced. The reconnection electric field and the vertical component of the magnetic field possibly cause a drift of hot electrons toward the earth, and this is projected to the polar ionosphere as the equatorward motion of the CNA band.

A very rough estimation of the energetic electrons' earthward drift speed and the intensity of the reconnection electric field can be made to explain the observed motion of the CNA band at a speed of ~500 m/s. If we assume that the mapping scale factor from the ground at 75° inv. to the magnetotail at ~25 R_E is a few hundred, the earthward drift speed of the energetic electrons would be ~100 km/s. This speed is smaller than the speed of the bursty bulk flow of several hundreds of km/s (Baumjohann *et al.*, 1990). If the earthward drift of the energetic electrons is caused by the E × B drift, a dawn-to-dusk directed electric field of a few hundreds of μV/m is required if we assume that the neutral sheet magnetic field intensity is ~2 nT.

5.2.4. Energetic electrons as a source of the equatorward-moving CNA band

A portion of the energetic electrons produced at the separatrix is thought to be the magnetospheric source of the equatorward-moving CNA band. These electrons are injected earthward across an L-shell by the reconnection electric field and trapped in the stretched fieldlines anchored to the earth. In the course of their passage across the L-shell, the energetic electrons gain energy by Betatron acceleration. The energy gain occurs in the perpendicular component and is proportional to the increase in the magnetic field intensity. If we assume that the magnetic field intensity just after the reconnection is ~2 nT (a typical neutral sheet magnetic field intensity) and that the dipolarized fieldline region is ~20 nT (a typical lobe magnetic field intensity), the energy gain by Betatron acceleration over the course of dipolarization would be about 10 times. Since this energy gain occurs in the perpendicular component, the pitch angle of the energetic electrons increases. Some kind of pitch angle scattering process is required for these electrons to precipitate and contribute to the increase in CNA activity.

On the other hand, as the fieldlines change from a very stretched pattern to a dipole-like configuration, the energetic electrons gain energy by Fermi acceleration. This energy gain occurs in the parallel component and is inversely proportional to the length of the fieldline in which the particle is trapped. If we assume that reconnection occurs at ~25 R_E and that the transition between the tail-like and dipole-like configuration occurs at ~10 R_E, the fieldline length just after reconnection would be ~60 R_E and the fieldline length at the transition point would be ~30 R_E. As a result, the energy gain from Fermi acceleration would be about 2 times over the course of dipolarization. The energy gain by Fermi acceleration is much smaller than that produced by Betatron acceleration. However, since the gain occurs in the parallel component, it makes a significant contribution to the precipitation of energetic electrons, resulting in an increase in CNA activity.

5.2.5. Persistence of equatorward moving CNA bands

When a new CNA band appears on the poleward side, the preceding CNA band moves equatorward and persists for several minutes. As discussed in Section 5.2.3, this CNA band is probably located in a closed fieldline region. The persistence of this CNA band suggests that the precipitation of energetic electrons continues for several minutes after the fieldline of interest has been reconnected. The trapped electrons mentioned in Section 5.2.4 might be a possible source of this CNA band. Electrons with a small pitch angle would precipitate into the ionosphere, causing CNA activity, and a loss cone would be formed in the velocity distribution function of the trapped electrons. As long as the fieldline is well stretched, the curvature radius of the fieldline would be very small at the far end of the magnetotail. This would cause pitch angle scattering of the trapped electrons in the energy range of several tens of keV, whose Larmor radius is comparable to the small curvature radius in the tail. The loss cone would be filled by the pitch angle diffusion, and precipitation would continue. The precipitation would stop when the fieldline was dipolarized and the minimum curvature along the fieldline became large enough to prevent the pitch angle scattering. The boundary of the fieldline curvature between the region of continuous pitch angle scattering and the stably trapped condition has been discussed by Sergeev and Tsyganenko (1982) and Sergeev and Malkov (1988) in connection with the isotropic boundary of precipitating electrons and ions in the polar upper atomosphere. They showed that the amplitude of scattering decreases rapidly when

the ratio R_C/ρ exceeds a certain value K, where R_C is the radius of the fieldline curvature and ρ is the effective gyroradius of a particle on the equator. K is usually valued at around 7.

The variation in R_C and ρ between a very stretched and a dipole-like fieldline configuration can be estimated. Energetic electrons of ~10 keV are produced in the reconnection. These electrons are accelerated by Betatron and Fermi accelerations to ~100 keV over the course of the dipolarization, as discussed in Section 5.2.2. This energy range is a typical energy responsible for producing CNAs. If the magnetic field intensity just after the reconnection is ~2 nT and increases to ~20 nT over the course of dipolarization, as discussed in Section 5.2.2, ρ_1 (for 10 keV and 2 nT) is 125 km just after reconnection and ρ_2 (for 100 keV and 20 nT) is 40 km in the dipolarized fieldline region. If R_C is smaller than 875 km (=7 ρ_1) at the reconnection site, pitch angle scattering would occur efficiently. In regions of dipolarized fieldlines, R_C is on the order of thousands of km, which is much larger than 280 km (=7 ρ_2), and pitch angle scattering will not occur. An isotropic boundary obviously exists between the two sites mentioned above, and the equatorward-moving CNA band will fade when it reaches this isotropic boundary.

6. Summary

The interhemispheric conjugacy of auroral poleward expansion was studied using conjugate imaging riometers at ~67° inv. (Syowa Station, Antarctica, and Tjornes, Iceland) and at 75–77° inv. (Zhongshan Station, Antarctica; Longyearbyen, Svalbard; and Danmarkshavn, Eastern Greenland).

(1) Ninety poleward expansion events were observed at ~67° inv. during 1992–1993. The results were analyzed, and the following conclusions were made.

(a) Apparent bimodal distribution of poleward expanding velocity

Two peaks in the poleward expansion velocity distribution are presented: a slow expansion with a velocity of 1–1.5 km/s at a polar ionospheric altitude of ~90 km, and a fast expansion with a velocity of 3–5 km/s. However, about 60% of the fast expansions are overestimated because the front of the CNA region is tilted, yet the observations of its motion are made using meridional beams. When the angle between the front and the meridian is reduced, the apparent poleward moving speed increases. If the events with a tilted front are removed from the calculation, the velocity distribution is no longer bimodal, but possesses a single peak at 1–1.5 km/s.

(b) Conjugacy of poleward expanding velocities

The expanding velocities at conjugate stations agree fairly well. The difference in velocity between the two stations remained within ±30% for half of the events. For the remaining events, the velocity ratio between the conjugate stations was distributed between 0.34 to 3.7 because of a slow expansion in one hemisphere and a fast expansion in the opposite hemisphere.

(c) Faster expanding velocity for Syowa

Although the velocity difference remained within ±30% for half of the events, the expanding velocity at Syowa was larger than that at Tjornes for 67% of the events.

The median value of this distribution is V_s/V_t =1.18 (Syowa is faster than Tjornes by 18%). An asymmetric configuration of the magnetic fields at the conjugate points (smaller dip angle and weaker total field at Syowa) is one possible reason for this phenomenon (see Section 3.2).

(d) Conjugate point location

The time lag in the passage of the CNA band over conjugate stations was typically between 30–60 s. The product of this time lag and the poleward expanding velocity gives the location of the actual conjugate point. For 87% of the total number of events, the conjugate point of Syowa was located within ±200 km of Tjornes. The conjugate point of Syowa was more often located equatorward of Tjornes (55%) than poleward (45%). These features are consistent with theoretical calculations of the conjugate points using Tsyganenko's 1989 model.

(2) Two case studies of poleward expansion at 75–77° inv. were performed. The first study involved a small high-latitude magnetic disturbance centered at 75° inv., while the second involved a substorm starting at 71° inv. and expanding to 76° inv. The poleward expansion at this latitude was characterized by a stepwise progression of CNA bands to higher latitudes. In other words, a new CNA band was formed 50–180 km poleward of the preceding band. A close relationship was seen between the appearance of a new CNA band and the equatorward motion of the preceding ones.

(3) The magnetospheric source of the equatorward moving CNA bands was considered. Energetic electrons formed at the reconnection site are injected earthward by the reconnection electric field. This motion can be seen at the foot of the fieldline as the equatorward motion of the CNA band. The energetic electrons gain additional energy from Betatron and Fermi acceleration as the fieldline in which the electrons are trapped dipolarizes. Just after the reconnection, the small curvature of the reconnected fieldline at the tail causes pitch angle scattering of the trapped electrons. The electrons that fall into the loss cone are then precipitated into the polar ionosphere, where they form a CNA band. The precipitation continues until the curvature of the dipolarized fieldline becomes much larger than the Larmor radius of the trapped electrons, halting the process of pitch angle scattering.

(4) Eighty-five CNA events observed at Longyearbyen over the period of January 27–April 7, 1997, were selected, and the appearance of conjugate CNA events in the Zhongshan and Danmarkshavn data was examined. Although the conjugate pair used at these latitudes was displaced longitudinally by ~500 km, conjugacy was generally good. If a time lag of ±15 min is allowed, 52% of the CNA events had a counterpart at Zhongshan and 40% had a counterpart at Danmarkshavn. This rather high level of conjugacy suggests that the characteristic longitudinal extent of the poleward expanding CNA bands is on the order of 500 km in the polar ionosphere.

Acknowledgments

The authors greatly appreciate the efforts of all those involved in the operation of the imaging riometers under harsh conditions at Danmarkshavn, Longyearbyen, Tjornes, Zhongshan Station and Syowa Station. The imaging riometer at Longyearbyen is operated by University Course in Svalbard (UNIS) as a scientific collaboration between

Danish Meteorological Institute and National Institute of Polar Research, Japan. One of the authors (H. Y.) would like to express his sincere appreciation to Mr. Kadokura for various discussions. We also thank the institutes that operated the IMAGE magnetometer array. Low-energy particle data from the Los Alamos National Laboratory (LANL) satellites and the interplanetary magnetic field data from the WIND satellite were obtained from ISTP key parameters provided by Dr. Belian, LANL and Dr. Lepping, Goddard Space Flight Center, NASA.

The editor thanks Dr. T. J. Rosenberg and another referee for their help in evaluating this paper.

References

Akasofu, S.-I. (1965): Dynamic morphology of auroras. Space Sci. Rev., **4**, 498–540.

Baumjohann, W., Paschman, G. and Luhr, H. (1990): Characteristics of high-speed ion flows in the plasma sheet. J. Geophys. Res., **95**, 3801–3809.

Birn, J. and Hesse, M. (1991): Substorm features in MHD simulations of magnetotail dynamics. Magnetospheric Substorms, ed. by J. Kan *et al.* Washington, D. C., Am. Geophys. Union, 177–190 (Geophys. Monogr. Ser., 64).

De la Beaujardiere, O., Lyons, L. R., Ruohoniemi, J. M., Friis-Christensen, E., Danielsen, C., Rich, F. J. and Newell, P. T. (1994): Quiet-time intensifications along the poleward auroral boundary near midnight. J. Geophys. Res., **99**, 287–298.

Detrick, D. L. and Rosenberg, T. J. (1990): A phased-array radiowave imager for studies of cosmic noise absorption. Radio Sci., **25**, 325–338.

Fujita, Y., Yamagishi, H. and Sato, N. (1998): Seasonal variation in the latitude of geomagnetically conjugate points observed with imaging riometers in the auroral zone. Nankyoku Shiryô (Antarct. Rec.), **42**, 1–19.

Hargreaves, J. K., Browne, S., Ranta, H., Ranta, A., Rosenberg, T. J. and Detrick, D. L. (1997): A study of substorm-associated nightside spike events in auroral absorption using imaging riometers at South Pole and Kilpisjaervi. J. Atmos. Solar-Terr. Phys., **59**, 853–872.

Hones, E. W., Jr., Pytte, T. and West, H. I., Jr. (1984): Association of geomagnetic activity with plasma sheet thinning and expansion: A statistical study. J. Geophys. Res., **89**, 5471–5478.

Kadokura, A., Aso, T., Sato, N., Haegstroem, I., Van Eyken, T., Brekke, A., Lorenzen, D. A., Moen, J., Hayashi, K., Smith, R. A. and Mukai, T. (1999): Coordinated study on the electrodynamics around the most poleward arc system of the double oval configuration in a substorm (1). 106th SGEPSS fall meeting, Sendai, Japan.

Lui, A. T. (1991): Extended consideration of a synthesis model for magnetospheric substorms. Magnetospheric Substorms, ed. by J. Kan *et al.* Washington, D. C., Am. Geophys. Union, 43–60 (Geophys. Monogr. Ser., 64).

McPherron, R. L., Russel, C. T. and Aubry, M. A. (1973): Satellite studies of magnetospheric substorms on August 15, 1968, Phenomenological model for substorm. J. Geophys. Res., **78**, 3131–3149.

Nielsen, E. (1980): Dynamics and spatial scale of auroral absorption spikes associated with the substorm expansion phase. J. Geophys. Res., **85**, 2092–2098.

Pudovkin, M. I. (1991): Physics of magnetospheric substorms: a review. Magnetospheric Substorms, ed. by J. Kan *et al.* Washington, D. C., Am. Geophys. Union, 17–27 (Geophys. Monogr. Ser., 64).

Sato, N. and Saemundsson, Th. (1987): Conjugacy of electron auroras. Mem. Natl Inst. Polar Res., Spec. Issue, **48**, 58–71.

Sergeev, V. A. and Malkov, M. V. (1988): Diagnostics of the magnetic configuration of the plasma layer from measurements of energetic electrons above the ionosphere. Geomagn. Aeron., **28**, 549–553.

Sergeev, V. A. and Tsyganenko, N. A. (1982): Energetic particle losses and trapping boundaries as deduced from calculations with a realistic magnetic field model. Planet. Space Sci., **30**,

999–1006.

Sergeev, V. A. and Yahnin, A. G. (1979): The features of auroral bulge expansion. Planet. Space Sci., **27**, 1429–1440.

Sergeev, V. A., Mitchell, D. G., Russell, C. T. and Williams, D. J. (1993): Structure of the tail plasma/current sheet at ~11 RE and its changes in the course of a substorm. J. Geophys. Res., **98**, 17345–17365.

Stauning, P. (1996): Investigation of ionospheric radio wave absorption processes using imaging riometer techniques. J. Atmos. Terr. Phys., **58**, 753–764.

Stauning, P., Yamagishi, H., Nishino, M. and Rosenberg, T. J. (1995): Dynamics of cusp-latitude absorption events observed by imaging riometers. J. Geomagn. Geoelectr., **47**, 823–845.

Tsyganenko, N. A. (1990): Quantitative model of the magnetospheric magnetic field: method and results. Space Sci. Rev., **54**, 75–186.

Tsyganenko, N. A. and Stern, D. P. (1996): Modeling the global magnetic field of the large-scale Birkeland current systems. J. Geophys. Res., **101**, 27187–27198.

(Received December 3, 1999; Revised manuscript accepted March 14, 2000)